ARTICLE

Facet-Resolved Electrochemistry of Polycrystalline Boron-doped Diamond Electrodes: Microscopic Factors Determining the Aqueous Solvent Window in Aqueous Potassium Chloride Solutions

Dan-Qing Liu,[a] Chang-Hui Chen,[a] David Perry,[a] Geoff West,[b] Sam J. Cobb,[c] Julie V. Macpherson*[a] and Patrick R. Unwin*[a]

Abstract: A systematic examination of the microscopic factors affecting the aqueous solvent (electrolyte) window of polycrystalline (p) boron-doped diamond (BDD) electrodes in chloride-containing salt solutions is undertaken using scanning electrochemical cell microscopy (SECCM), in conjunction with electron backscatter diffraction (EBSD) and Raman microscopy. A major focus is to determine the effect of local boron doping level, within the same orientation grains, on the solvent window response. EBSD is used to select the predominant (110) orientated areas of the surface with different boron-doped facets, thereby eliminating crystallographic effects from the electrochemical response. Voltammetric SECCM is employed, whereby a cyclic voltammogram (CV) is recorded at each pixel mapped by the meniscus-contact SECCM cell. The data obtained can be played as an *electrochemical movie* of potential-resolved current maps of the surface to reveal spatial variations of electroactivity, over a wide potential range, including the solvent (electrolyte) window. Local heterogeneities are observed, indicating that the solvent window is mainly linked to local dopant levels, with lower dopant levels leading to a wider window, i.e. slower electrode kinetics for solvent/electrolyte electrolysis. Furthermore, the effects of O- and H-surface termination of the BDD surface are investigated, for the same electrode (in the same area). The surface termination is a particularly important factor: the solvent window of an H-terminated surface is wider than for O-termination for similar boron dopant levels. Further, the anodic potential window of the O-terminated surface is greatly diminished due to chloride electro-oxidation. These studies provide new perspectives on the local electrochemical properties of BDD and highlight the importance of probing the electrochemistry of BDD at the level of a single crystalline grain (facet) in order to unravel the factors that control the solvent (aqueous) window of these complex heterogeneous electrodes.

Introduction

Conductive boron doped diamond (BDD) is gaining remarkable interest as an electrode material for electrochemical studies and applications, particularly in aqueous solutions, due to properties such as wide solvent (electrolyte) window, low background current, reduced susceptibility to fouling, chemical inertness and mechanical durability.[1] The solvent (electrolyte) window defines the potential range over which an electrode can be used for voltammetric/amperometric detection of solute molecules (analyte), without significant impact from electrolysis of either the solvent or supporting electrolyte. For water, this often constitutes the oxygen evolution reaction (OER) at anodic potentials and the hydrogen evolution reaction (HER) at cathodic potentials, although the electrolyte itself can also have an influence, as examined herein.

Compared to other carbon-based and metallic electrodes, BDD presents a wider solvent window in aqueous solution, allowing the detection of various analytes at extreme potentials,[2] and opening up novel applications in electroanalysis and electrode functionalization.[3] On BDD, water oxidation by the conventional OER route is strongly retarded and oxidation can occur via an alternative pathway, which results in production of the hydroxyl radical ($OH^{\cdot}$).[4] As a consequence, BDD electrodes are used widely for electrochemical water treatment (formation of $OH^{\cdot}$ desirable), while BDD itself is resistant to $OH^{\cdot}$ attack.[5] In the presence of chloride, oxidation to chlorine may also define the anodic window.[6]

Although the wide solvent window is a well-known electrochemical characteristic of polycrystalline (p) BDD, the effect of intrinsic microscopic factors on this property, including crystallographic orientation, boron dopant concentration, and surface termination within this complex heterogeneous material are much less well understood. The surface of freshly grown BDD is hydrogen (H)-terminated and hydrophobic, but slowly air oxidizes to the oxygen (O)-terminated form.[7] As outlined below, most studies have relied on macroscopic measurements to probe these factors, which can be restrictive in terms of obtaining microscopic insight. During the growth of pBDD, different crystal facets (grains) take up boron to different extents,[8] and thus the BDD electrode presents a heterogeneously doped surface, making microscopic characterization measurements essential.

For macroscopic measurements of pBDD, it has been reported that the solvent window decreases slightly as the boron doping level increases,[9] and this effect is more marked on the cathodic side.[10] However, others report no effect of boron doping and instead show the importance of sp^2 content, with the window narrowing with increasing sp^2 content of the electrode surface.[11] sp^2 carbon has also been shown to catalyze water electrolysis[9, 12] resulting in both a measurable oxygen reduction reaction (ORR) signal[9] and features in the anodic window just before the

[a] D. Liu, Dr. C. Chen, Dr. D. Perry, Prof. J. V. Macpherson, Prof. P. R. Unwin
Department of Chemistry
University of Warwick
Coventry, CV4 7AL, UK
E-mail: j.macpherson@warwick.ac.uk; P.R.Unwin@warwick.ac.uk
[b] Dr. G. West
Warwick Manufacturing Group
University of Warwick
Coventry, CV4 7AL, UK
[c] S. J. Cobb
Centre for Doctoral Training in Diamond Science and Technology
University of Warwick
Coventry, CV4 7AL, UK

onset of water oxidation.[13] There is also a report that the surface orientation of BDD influences the solvent window, attributed to different electrode kinetics on the different crystal faces of BDD.[14] However, as the boron concentration also changes within different crystal planes exposed on the BDD surface, it is not possible to distinguish between doping and surface orientation effects from these reported measurements.[15] The effect of surface termination has also been investigated, with the solvent window response of H- and O-terminated (prepared e.g. by oxygen plasma,[16] acid boiling[17]) surfaces compared.[16] In sulfate media, the solvent window was found to be larger on O-BDD than H-BDD.[16b]

High-resolution correlative electrochemical imaging methods have provided considerable information for different outer sphere redox couples (on different surface terminations), and both inner sphere and more complex proton-coupled electron transfer processes, on individual grains and defects of pBDD.[18] Such approaches therefore have considerable prospect to elucidate some of the key microscopic factors determining the solvent window of BDD directly. In this paper, we use voltammetric SECCM,[19] combined with electron backscatter diffraction (EBSD) and Raman microscopy, applied to the same areas of a BDD electrode, to investigate how the local properties of BDD surfaces influence the aqueous solvent window in chloride media and identify the factors that are most important. We use a chloride supporting electrolyte for these studies, as it is used commonly in electroanalytical measurements and in real world applications, e.g. electroanalytical/disinfection measurements in seawater,[20] and it presents a competing pathway to OER for control of the anodic potential window.

Results and Discussion

Voltammetric SECCM. Figure 1 illustrates voltammetric SECCM setup (Figure 1a) used in this work.[19c, 21] Briefly, a theta pipet (Figure 1(b)), filled with 50 mM KCl, contained quasi-reference counter electrodes (QRCEs) in each channel, functions as a microelectrode. The pipet was approached toward the BDD surface until the meniscus made contact (the pipet itself not making contact). The method allows (multiple) CVs to be recorded at individual pixels in an area of interest on the BDD substrate. The details are described in the experimental section.

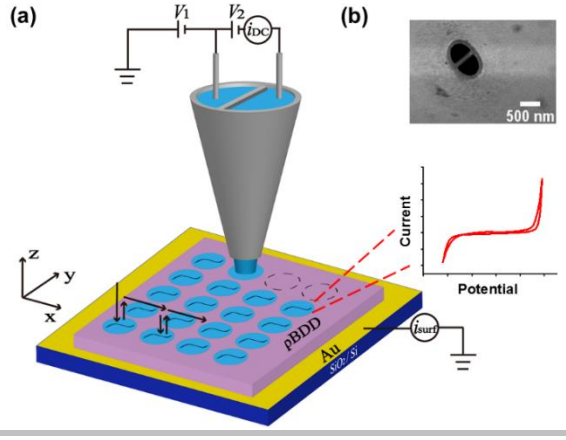

Figure 1. (a) Schematic of voltammetric SECCM. The blue circles on the pBDD surface represent the probed areas and constitute an individual pixel, as described in the text. A 10 V s^{-1} scan rate was used for the CVs at each pixel (inset response). (b) Field emission scanning electron microscopy image of the end of a typical pipet used for SECCM.

EBSD characterization of BDD electrodes. In this study, BDD was grown using microwave plasma-chemical vapor deposition (MW-CVD) under conditions which produce the highest quality electrodes for electrochemistry, minimizing sp^2 carbon content (grown using very similar procedures to that used to produce electrode E in reference 9). Crystallographic orientation information of the areas studied by electrochemical imaging (*vide infra*) was obtained by EBSD. Typical data are shown in Figure 2(a). EBSD demonstrates that the majority of the surface, post-polishing, has an orientation of (110), with a minor contribution from (100).[22]

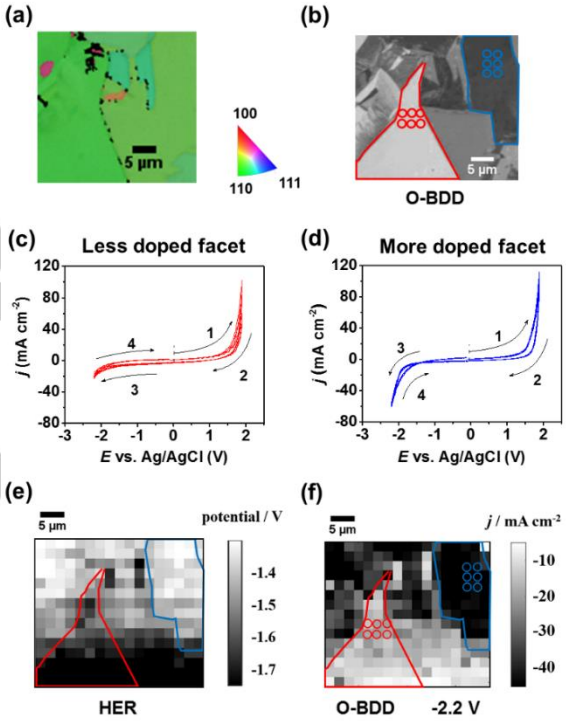

Figure 2. (a) EBSD and (b) corresponding FE-SEM image of area I on the pBDD electrode. The orientation maps in (a) are colour-coded according to the growth direction. The facet with the red boundary in (b) denotes a less doped grain, whilst that in blue represents a more doped grain. Six individual CVs (overlaid) recorded in different locations on an O-terminated surface in each of (c) the less doped facet (red circles) and (d) the more doped facet (blue circles). The numbers and arrows highlight the scan start potential and scan directions. (e) SECCM onset cathodic potential image of area I for a current density of -3.5 mA cm^{-2}. (f) SECCM current density image of area I at -2.20 V.

Raman characterisation of BDD electrodes. Raman mapping, as detailed in Supporting Information (Section S1), was used to assess the boron concentration and the material sp^2 content. The Raman spectra showed a Fano resonance on both low and high doped grains (Figure S1(b)-(d)) indicating the material is degenerately doped and metallic in nature. The 500 cm^{-1} peak is often present in heavily doped BDD and shifts to lower wavenumbers with increasing boron concentration. This peak can be used to empirically assess the boron doping

concentration,[23] with the shift suggesting a factor of ten difference in boron concentration between the highest and lowest doped grains, for which we investigate the electrochemistry.

The ratio of sp^2/sp^3 features i.e. the intensity of the G-band (the broad peak around 1550 cm^{-1}) to that of the diamond peak (1322-1333 cm^{-1}) was found to be spatially heterogeneous, ranging from 0.016-0.12.[15a, 24] This suggests the sp^2 content is low in all grains. Grains with low dopant density have the lowest apparent sp^2 levels, and those with high dopant density, have a wider spread of slightly higher sp^2 levels. It should be noted, however that the diamond peak varies in intensity and position with boron doping level,[25] decreasing in intensity and shifting to lower wavenumbers as boron doping increases. The increased size of the diamond peak in low doped samples can explain the apparent lower sp^2 content in lower doped grains and therefore quantification should be treated carefully. However, it is valid to comment that the sp^2 content is low in all regions. Finally, it is important to note that although Raman microscopy reveals a heterogeneous distribution of sp^2 carbon across the BDD electrode, the Raman signal represents information from the surface down to several microns into BDD,[26] and therefore is not necessarily a true reflection of surface sp^2 carbon, unlike electrochemical signals.[27]

Voltammetric SECCM at O-BDD electrode. The O-BDD surface is hydrophilic, with an aqueous contact angle value of 26° (Supporting Information (SI), Section S2). As a consequence, the SECCM approach adopted, where meniscus contact at each position was brief (< 1 s; *vide supra*) served to prevent extensive local wetting of the surface (from leakage of solution from the tip). Figure 2(b) is an field emission scanning electron microscopy (FE-SEM) image of area I (34 × 30 μm). Darker regions in the FE-SEM image correspond to the more boron doped regions while lighter zones present the less boron doped regions,[28] in agreement with the Raman mapping *vide supra*.

SECCM CVs were recorded on area I, at each pixel, at a scan rate of 10 V s^{-1}, starting from a position left bottom, and progressing in a raster pattern to top right. All the SECCM scans were performed in air with a 2 μm pixel-pitch, equivalent to 255 individual CVs and a total imaging time of 53 mins (0.82 s per CV with the meniscus in contact with the surface). Although surface termination modification is highly unlikely under the conditions of our experiment (very short residence times at potentials ≥ ± 1 V, the avoidance of acidic solutions), to further ensure negligible O-termination disruption, which may possibly result from electrochemical cathodic treatments (due to partial conversion to H-termination),[29] CVs started at -0.1 V, with the potential scanned anodically to 1.9 V, then reversed back to -2.2 V, before finally scanning again to -0.1 V. Regions with very similar doping levels, as identified from the FE-SEM image, and recorded in the earlier and latter part of the scan, gave very similar CV responses. This indicated that the BDD sample was not adversely affected by being in the ambient atmosphere, prior to contact with the electrolyte droplet.

Table 1. Table of solvent window of O-BDD (area I) and H-BDD (area I').

Surface	Doped facet	Onset potential		Solvent window
		E_{anodic} (V)	$E_{cathodic}$ (V)	ΔE (V)
O-BDD	Less	1.05 (±0.089)	-1.74 (±0.13)	2.79 (±0.22)
	More	1.00 (±0.052)	-1.39 (±0.083)	2.34 (±0.12)
H-BDD	Less	1.88 (±0.090)	-2.16 (±0.072)	4.04 (±0.15)
	More	1.54 (±0.11)	-1.97 (±0.082)	3.52 (±0.20)

*Values were obtained from all pixels in the representative most and least doped facets as marked in Figure 2(b) and Figure 3(a.)

Twelve typical CVs (six in each facet), in the least doped (indicated by the red circles in Figure 2(b)) and most doped facet (blue circles in Figure 2(b)) are shown in Figures 2(c) and 2(d). It can immediately be seen that the doping level has a strong effect on the cathodic window, in particular, with the most doped grains being most electrocatalytic, as we highlight further below. Note that current densities were calculated based on a measured circular wetting area diameter, $d = 1.94 \pm 0.06$ μm, using the mean value. d was estimated from the meniscus residues of 86 representative pixels analyzed by FE-SEM, as detailed in the Supporting Information (SI, Section S3). Within error, the meniscus wetting was independent of boron doping level.

In these twelve microscale CVs, only a double layer region between the solvent window defining anodic and cathodic processes was observed. There was no evidence of an electrochemical sp^2 carbon signal or an oxygen reduction current[9] and no apparent link can be drawn between the solvent window magnitude and the sp^2 levels from Raman microscopy for the higher doped grains (compare the doping level data (image) in Figure 2(b), electrochemical image in Figure 2(e) to the Raman image in SI, Figure S1(a)). These observations further supported the conclusion that any sp^2 contributions to the electrochemistry are insignificant.

The current densities, j, reported in literature to define the solvent window of BDD, range from 0.25 mA cm^{-2} to 2 mA cm^{-2} (at 0.1 V s^{-1}).[9, 12, 30] Here, we use 3.5 mA cm^{-2}, because the high scan rates (10 V s^{-1}) employed during our CV analysis, gave an appreciable capacitive current (~2.5 mA cm^{-2}). The value of 3.5 mA cm^{-2} is sufficiently above this background contribution by ca. 1 mA cm^{-2}, which is in the middle of the range defined above for identifying the solvent window. SECCM onset potential maps both for the cathodic and anodic processes are plotted by extracting potential values of every pixel at -3.5 mA cm^{-2} and +3.5 mA cm^{-2}. In Figure 2(e), the SECCM onset potential map for the cathodic process has a strong correlation with boron doping level that can be gleaned from the contrast in the FE-SEM image in Figure 2(b), with lower doped facets appearing brighter.[28] It is evident that the more doped facets have a less negative onset potential than the lower doped facets. In contrast, for the anodic process, the onset potential for the higher and lower doped facets is, within error, more or less the same (SI, Section S4). Values for the solvent window and the cathodic/anodic onset potentials, are summarized in Table 1. Note that these values are averages of all

pixels recorded in each of the least doped facets (47 pixels for O-BDD and 32 pixels for H-BDD) and most doped facets (47 pixels for O-BDD and 62 pixels for H-BDD) as marked with red and blue lines (Figure 2(b) for O-BDD and Figure 3(a) for H-BDD). As Table 1 shows, for O-BDD, the solvent window of the less doped facet is 45 mV wider than that of the more doped facet, due to differences in the onset potential for the cathodic process.

To further illustrate the difference of cathodic activity across the scanned area, the surface current, i_{surf}, at a potential of -2.2 V (the maximum cathodic potential investigated), was extracted and plotted as an image, as shown in Figure 2(f). Clearly, there is a correlation between the SECCM image (Figure 2(f)) and the FE-SEM image (Figure 2(b)), with the lower doped regions showing lower current densities in the cathodic region. The darkest regions in the FE-SEM image, which correspond to the most highly doped regions,[28] show the largest current densities.

The full movie comprising current images with a step of 10 mV between each generated current map (820 different potentials/maps across the forward and reverse scan), is shown in Supporting Information, Movie S1. The movie represents the electrochemical activity of the electrode surface as a function of the applied working electrode potential, and highlights that spatial heterogeneities in anodic and cathodic activity appear at the most extreme potentials, near the solvent windows, in line with the CVs described above. The same correlative multi-microscopy approach was executed on another area (area II) of the same O-BDD electrode (SI, Section S5). The results were similar to those presented herein, i.e. the local boron doping level affected the onset potential for the cathodic process but not the anodic one.

Macroscopic studies of the solvent window in several supporting electrolytes including chloride solutions, for differently doped nanocrystalline O-BDD electrodes (anodically treated in acid) have been reported.[10] It was also found that the solvent window decreased as the *average* boron doping level increased, and the cathodic onset potential was affected more by doping than the anodic one. However, changes in the anodic onset potential were still observed.[10] In these studies, measurements were averaged across a geometric area of 5.72 mm,^{2} and were thus unable to take account of heterogeneity in doping of the surface. In contrast, we have been able to make 255 individual measurements, all at different locations, with the electrochemical response correlated to the properties of individual grains/facets.

Voltammetric SECCM at H-BDD electrode. To explore the impact of surface termination on the solvent window of BDD, the O-BDD electrode was H-terminated using a hydrogen plasma treatment,[16a] resulting in a water contact angle of 86° (SI, Section S2). Voltammetric SECCM scanning at the H-BDD electrode was carried out in a region containing the same facets as area I (Figure 2(b)), 24 × 40 µm, marked as I' in the FE-SEM image in Figure 3(a). Again, to minimize oxidation of the H-BDD surface during potential cycling, CVs started at a potential of -0.1 V, with the potential scanned cathodically to -2.2 V, then reversed to 2.2 V and finally back to -0.1 V.

An FE-SEM image of the meniscus residues after scanning is shown in Supporting Information (SI, Section S6). The diameter

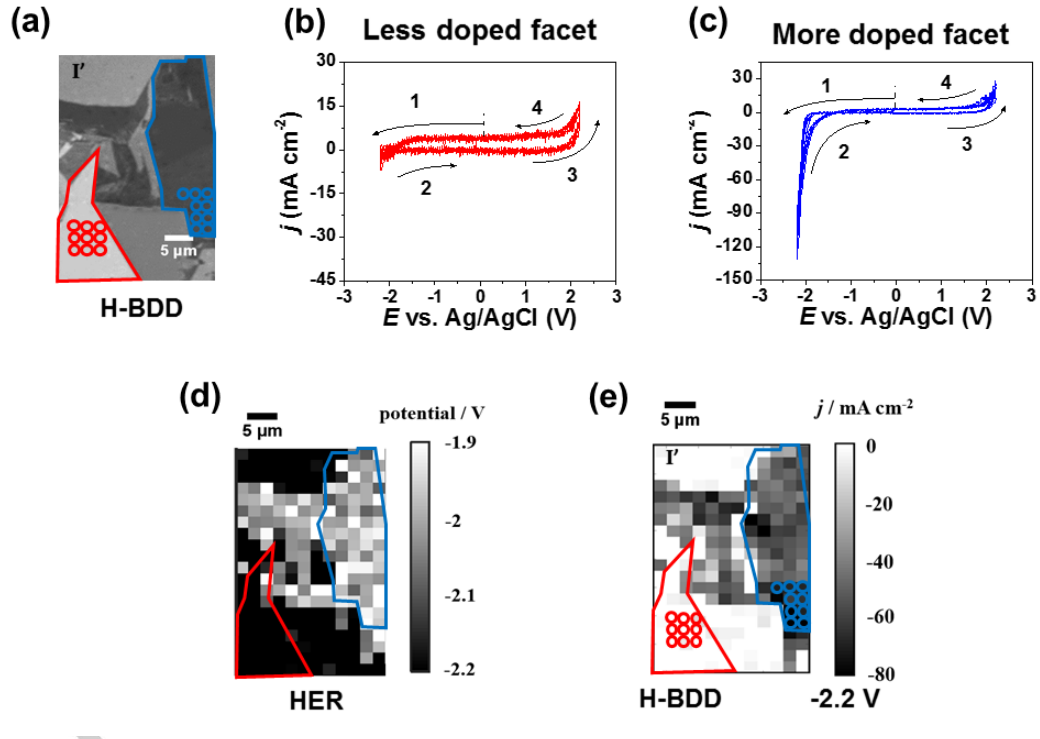

Figure 3. (a) FE-SEM image of area I'. (b-c) Corresponding individual CVs for less doped facet (9 individual CVs corresponding to the red circles in a) and more doped facet (9 individual CVs corresponding to the blue circles in a). Note the different current scales in these plots. (d) SECCM onset cathodic potential image of area I' for a current density of -3.5 mA cm^{-2}. (e) SECCM current density image of area I' at -2.20 V.

of the meniscus was found to be 696 ± 52 nm (obtained from 118 pixels), much smaller than that on O-BDD (*vide supra*), due to the hydrophobic nature of H-BDD. The meniscus wetting was also found to be independent of doping level (SI, Section S6).

Eighteen typical CVs (nine in each facet) on a less doped (indicated by the red circles in Figure 3(a)) and more doped facet (blue circles in Figure 3(a)) are shown in Figures 3(b) and 3(c). The SECCM onset potential image for the cathodic process (assuming a current density of -3.5 mA cm^{-2} which was about 1 mA cm^{-2} in magnitude greater than the background cathodic level of ~ -2.5 mA cm^{-2}) is displayed in Figure 3(d). The onset potential of the less doped facet is -190 mV more negative than that for the more doped facet (broadly similar to what was found for the O-BDD surface; *vide supra*). However, in contrast to the behavior for the O-BDD surface, on H-BDD the anodic process occurs at a potential value that is 340 mV more positive for the less doped (SI, Section S4) than the more doped facet. Furthermore, compared to O-BDD, on H-BDD the solvent window is significantly larger by 1250 mV on the less doped facet and by 1170 mV on the higher doped grain. The solvent window and onset potential analysis for both the anodic and cathodic processes are summarized in Table 1.

To illustrate the facet dependence of the cathodic process activity, an SECCM map at an applied potential of -2.2 V (again representing the maximum applied cathodic potential), selected from potential resolved images, is shown in Figure 3(e). Clearly, there is a strong correlation between the electrochemical activity image (Figure 3(e)) and the corresponding facets in the FE-SEM (Figure 3(a)), with the more doped facets yielding a higher current density than the less doped facets. A movie of the electrochemical current for the H-BDD surface as a function of potential is given in SI, Movie S2. As for the O-BDD surface, spatial heterogeneities in the activity are evident at the most extreme potentials.

As for the O-BDD experiments, a different area of the H-BDD surface (area II', similar region to area II, *vide supra*) was studied. The results are summarized in SI, Section S7 and are in agreement with the data presented herein.

Processes defining the solvent window. Examining the results of Figures 2 and 3, summarized in Table 1, the solvent window is found to be wider for H-BDD than O-BDD. For O-BDD, decreasing the doping level increases the onset potential for the cathodic process, whilst the anodic onset potential stays more or less the same. For H-BDD, both the anodic and cathodic onset potentials increase as the boron doping level decreases.

Considering the cathodic process, the HER controls the current on both surface-terminations of BDD. On diamond electrodes, the reaction is considered to proceed via proton discharge in the presence of a surface adsorbed H radical to produced H_2[31] (Volmer-Heyrovsky mechanism) i.e.

$$C\text{-}H + H^+_{(aq)} + e^- \rightarrow C^{\cdot} + H_2 \qquad (1)$$

In contrast for the anodic process, in chloride containing solution, there is competition between OER (equation 2, 3) and chloride oxidation (equation 4).

For OER, the conventional processes, i.e.

$$2H_2O \rightarrow O_2 + 4H^+ + 4e^- \qquad E^o = 1.23\ V \qquad (2)$$

is not catalytically favoured on BDD[32] and at the extreme electrode potential defining the anodic window, the following can also take place

$$H_2O \rightarrow OH^{\cdot} + H^+ + e^- \qquad E^o = 2.73\ V \qquad (3)$$

Additionally, chloride oxidation to chlorine is a consideration:

$$2Cl^- \rightarrow Cl_2 + 2e^- \quad E^o = 1.36\ V \qquad (4)$$

Our finding of a wider solvent window for H-BDD compared to O-BDD contrasts with previous literature on macroscopic electrodes where the opposite has been seen.[16b] The O-BDD electrodes in the literature studies[16] were O-terminated using an oxygen plasma treatment (whereas we use a strong acid clean) and measurements were made in either acidic sulfate solutions[16b] or PBS buffer solutions.[16a] Sulfate can be oxidized to $S_2O_8^{2-}$, but only at very high anodic potentials on BDD electrodes.[33] For the PBS buffer solutions, the electrolyte ions used are inert, and the anodic process is driven by OER and the cathodic process by HER. Additionally, macroscopic voltammetric measurements on very similar O-BDD material as used by us, but in nitrate media, report a solvent window of 3.6 V for O-BDD,[9] wider than reported here; note only OER is present anodically (via eqs 2 and 3).

The diminished anodic window that we observe on O-BDD, in chloride solution, indicates that chloride oxidation must play a significant role in defining the onset anodic potential. This is confirmed by comparing the solvent window response of a O-BDD macroelectrode (1 mm diameter and very similar material quality to that used herein) in several different electrolytes (0.1 M KCl, KNO_3 and K_2SO_4) as shown in Supporting Information (SI, Section S8). The anodic solvent window is very similar for sulfate versus nitrate; although for sulfate there is a pre-wave prior to the main oxidative current. The origin of this feature has been discussed in some detail in reference [33a]. However, the onset anodic potential in chloride media is greatly diminished due to chloride oxidation. Evidently, our microscopic data indicate that for the range of boron-doping levels in the pBDD electrodes used by us, the onset potential for the chloride oxidation process is not appreciably affected by the boron dopant density in these BDD electrodes.

In comparison to O-BDD, the much larger anodic onset potential on H-BDD indicates that chloride oxidation must be significantly kinetically hindered on this hydrophobic surface. Moreover, the very large shift in the anodic onset potential for H-BDD means that on the H-BDD surface OER, via equation (3), would (at least partly) contribute to the current. Indeed, a switch in the oxidation pathway from chloride oxidation to OER is also suggested by the fact that for the H-terminated surface, the anodic onset potential is dependent on the boron dopant density, whereas there is little such dependence for the O-BDD surface. This is a very interesting observation for which further experimental and theoretical studies could usefully aid understanding.

The level of local boron doping in pBDD has a number of consequences, including affecting the local density of electronic states and the number of boron atoms in the (sub) surface region. Evidently, increasing boron levels in BDD decreases the onset potential for HER on both O-BDD and H-BDD electrodes, as well as the anodic process on the H-BDD surface. For HER, weakly

adsorbed H radicals on the surface of the BDD (formed by the transfer of an electron to H^+) are thought to be important in the overall hydrogen discharge process. Calculations[31] have shown that the presence of sub surface C-B bonds has an impact on weakening the bond between an electrochemically formed H radical and the carbon surface, promoting further reaction of this radical with H^+ to form H_2, which explains the diminished overpotential in the higher doped grains (compared to lower doped grains) of both H-BDD and O-BDD. Our data further suggests this process is favored by O-termination of the surface. For the H-terminated surface, where we propose the OER via eq 3 plays a role, such factors could also be important, especially if the adsorption of water on the surface is a limiting step in the process. Further theoretical work is needed to understand these processes in greater detail, and microscopic measurements such as those herein, will aid the development of a deeper understanding.

Conclusions

Voltammetric SECCM, which combines SECCM imaging with a CV measurement at each pixel, has proven powerful in highlighting key surface processes that affect the local solvent window of pBDD with both hydrogen and oxygen terminations in chloride solutions. A key feature of this approach is that CVs are recorded at hundreds of spots for correlation between electrochemistry and structure effects, to unambiguously identify correlation between various local material properties of the electrode and the electrochemical activity.

In this work, we have used correlative electrochemical microscopy to investigate the impact of boron dopant concentration and electrode surface termination on the solvent window of BDD. Voltammetric SECCM has revealed that the solvent window is directly linked to the local boron dopant concentration, irrespective of the surface termination, with the solvent window for less-doped facets being wider than for more-doped facets. However, it is noteworthy that the onset potential for the anodic process is relatively insensitive to boron doping level for O-BDD (for the doping levels herein), but doping dependent on H-BDD. This is proposed to be due at least in part to a change in the mechanism to OER, rather than chloride oxidation on the H-BDD. However, further work to probe the processes involved in the anodic processes at the different electrodes is needed. Scanning electrochemical microscopy (tip collection measurements) could be very useful in this regard to attempt to detect the products and intermediates of the electrode process. On both surfaces, the cathodic onset potential is governed by the HER and this is more facilitated at O-terminated surfaces and surfaces of higher boron-doping density.

The results provided by this study are valuable for designing and optimising electrodes where a particular solvent window is desired or, with further direct confirmation, where a particular reaction in the anodic window is required, for example for water treatment or electrosynthesis. Both the boron dopant concentration and surface termination are key factors that can be tuned to achieve particular properties for practical electrodes, and this study has highlighted how multiple measurements at the single entity (BDD facet) level are particularly powerful in elucidating the overall properties of a complex macroscopic electrode.

Experimental Section

Chemicals and materials. Potassium chloride (KCl, ACS reagent grade, Sigma Aldrich) was used as a background electrolyte, and concentrated sulfuric acid (H_2SO_4, > 95 %, Fisher Chemicals) and potassium nitrate (KNO_3, ACS reagent grade, Sigma Aldrich) were employed for BDD cleaning. 50 mM KCl electrolyte solutions were prepared immediately prior to use. All aqueous solutions were prepared from ultrapure water (SELECT-HP, Purity, 18.2 MΩ cm resistivity at 25 °C). Silver-chloride coated silver wires (Ag/AgCl) were used as QRCEs for SECCM. All potentials reported for SECCM herein are against the Ag/AgCl QRCEs, which had a stable potential of 59.60 mV (at a temperature of 298 K) vs. saturated calomel reference (SCE) in 50 mM KCl. As reported elsewhere,[34] this QRCE functions as a very stable electrode over long time periods in SECCM.

Preparation of BDD samples. The BDD electrode (350 μm thick) was grown using a commercial MW-CVD process (Element Six, Harwell, UK) to be metal-like doped[1a, 9] and the surface was mechanically polished to sub nm surface roughness.[9] Prior to use, the freestanding BDD was cleaned by heating in a concentrated H_2SO_4 (> 95 %) solution containing saturated KNO_3 solution at 300 °C for 30 minutes. This also resulted in O-termination of the surface.[28] For H-BDD studies, the surface was H-terminated using a hydrogen plasma CVD reactor, heated at 1 kW under 60 Torr of H_2 for 10 min. After that, the CVD reactor was powered down, and H_2 was continually passed over the surface at a flow rate of 500 cm^3 min^{-1} for another 10 min.

The back side of the BDD was sputtered (Moorfield) with Ti/Au (10 nm/300 nm) and then annealed in a tube furnace (Carbolite, U.K.) at 400 °C for 5 hours to form an ohmic titanium carbide contact.[1a] A conducting connection to the BDD was made by attaching the sample to a Ti/Au (10/300 nm) sputtered Si/SiO_2 wafer, using silver paint (Agar Scientific, Ltd, U.K.), electrically connected using a copper wire. Prior to electrochemical studies, the electrode was marked, using laser-cut crossed lines of ca. 14 μm width (E-355H-ATHI-O system, Oxford Lasers Ltd.), for ease of finding the same scanned area in SECCM and with other microscopic measurements (correlative microscopy).

Pipet fabrication. Pipets used were pulled from borosilicate theta capillaries (Harvard Part No.30-0114), using a Sutter P-2000 laser puller (Sutter Instruments, USA). After pulling, the inner diameters of the end of the pipets were in the range 700 - 900 nm, with the dimension determined accurately by field-emission scanning electron microscopy (FE-SEM, Zeiss SUPRA 55). To confine an aqueous meniscus to the very end of the pipet, the outer walls were silanized by placing the probe in dichlorodimethylsilane (99+ % purity, Acros), with argon flowing through to protect the inside from silanization.

Voltammetric SECCM setup. A bias voltage, V_2 (200 mV), was applied between the QRCEs to generate an ion conductance current (i_{DC}). Modulation of the z position of the pipet (266 Hz, 50 nm peak amplitude) by a lock-in amplifier (Stanford Research, SR830) generated an AC component of the ion conductance current, i_{AC}, at the modulation frequency. This was used for positional feedback[35] to detect when meniscus contact with the BDD surface was made via the probe. The potential of the BDD electrode was controlled by varying the potential

applied to one of the QRCEs (V_1), and was – (V_1+V_2/2) vs. Ag/AgCl QRCE; see Figure 1(a).[36] Current that flowed through the substrate, which served as the working electrode, is denoted as i_{surf}.

An approach-hold-withdraw (hopping) mode[19c] was employed for measurements at each pixel, as shown in Figure 1(a). First, the pipet approached the BDD surface at a speed of 0.2 μm s^{-1}. Once meniscus contact was established, the pipet was held fixed in position for 0.1 s, before CV measurements at a sweep rate of 10 V s^{-1}, resulting in < 1 s measurement time for each pixel even over the wide potential range of these measurements (*vide infra*). The pipet probe was then retracted away from the surface at a speed of 2 μm s^{-1} by a distance of 2.5 μm, and then by 2 μm in the *xy* plane laterally to a neighboring pixel, where the same measurement procedure was implemented. This protocol was repeated until all the pixels in the area of interest were covered. The short residence time at each pixel minimized the chance of substrate wetting (meniscus spreading), especially for O-BDD, a very hydrophilic surface.

The current, i_{surf}, plotted against the corresponding *xy* position, as a function of potential, generated a sequence of SECCM image frames that constituted a potentiodynamic movie. The movies obtained, contained 820 frames, with a potential resolution of 10 mV (see, for example, Supporting Information, Movie S1 and S2, which are referred to herein). All data analysis was performed with Matlab (R2014b, Mathworks).

Structural characterization. *EBSD*. The crystal orientation of the polished pBDD for the SECCM scanned areas was determined by FE-SEM: Zeiss SUPRA, with a Nordlys F (Oxford Instruments) camera. EBSD measurements were performed with a pixel spacing of 0.3 μm at 20 kV, with the BDD electrode tilted at 70°. Data were analyzed using Aztec 3.1 (Oxford Instruments).

FE-SEM. The scanned areas including any droplet residues, were imaged using a Zeiss SUPRA 55 FE-SEM, at 5 keV with the inlens mode.

Contact angle measurements. Static contact angle measurements[37] were performed on a Krüss DSA 100 by depositing a volume of ~5 μL deionized water on the BDD surface.

Raman mapping. Raman microscopy mapping was performed using a Renishaw InVia micro-Raman spectrometer, with a diode-pumped solid-state laser (excitation wavelength of 532 nm). Spectral acquisition was performed at 100 % power with an integration time of 10 s. A step size of 0.6 μm was chosen for Raman mapping.

Acknowledgements

The authors thank Ashley Page for writing MATLAB programs used to analyse the Raman map data herein, and Minkyung Kang for helpful discussions. PRU and JVM thank the Royal Society for a Wolfson Research Merit Award and Industry Award, respectively. DQL thanks the China Scholarship Council-Warwick joint scholarship programme. CHC thanks the U.K. Catalysis Hub for financial support. The UK Catalysis Hub Consortium is funded by EPSRC (grants EP/K014706/2, EP/K014668/1, EP/K014854/1, EP/K014714/1 and EP/M013219/1).

Keywords: scanning electrochemical cell microscopy • boron doped diamond • solvent window • boron doping level • surface termination

[1] a) J. V. Macpherson, *Phys. Chem. Chem. Phys.* **2015**, *17*, 2935-2949; b) H. B. Martin, A. Argoitia, U. Landau, A. B. Anderson, J. C. Angus, *J. Electrochem. Soc.* **1996**, *143*, L133-L136; c) J. V. Macpherson, *The Use of Conducting Diamond in Electrochemistry, Vol. 16* (Wiley-VCH Verlag GmbH & Co. KGaA, Weinheim, Germany) **2015**, pp. 163-210.

[2] B. Sarada, T. N. Rao, D. Tryk, A. Fujishima, *Anal. Chem.* **2000**, *72*, 1632-1638.

[3] a) J. Svítková, T. Ignat, Ľ. Švorc, J. Labuda, J. Barek, *Crit. Rev. Anal. Chem.* **2016**, *46*, 248-256; b) A. Härtl, E. Schmich, J. A. Garrido, J. Hernando, S. C. Catharino, S. Walter, P. Feulner, A. Kromka, D. Steinmüller, M. Stutzmann, *Nat. Mater.* **2004**, *3*, 736-742; c) M. Medina-Sánchez, C. C. Mayorga-Martinez, T. Watanabe, T. A. Ivandini, Y. Honda, F. Pino, K. Nakata, A. Fujishima, Y. Einaga, A. Merkoçi, *Biosens. Bioelectron.* **2016**, *75*, 365-374.

[4] a) B. Marselli, J. Garcia-Gomez, P.-A. Michaud, M. Rodrigo, C. Comninellis, *J. Electrochem. Soc.* **2003**, *150*, D79-D83; b) P. Michaud, M. Panizza, L. Ouattara, T. Diaco, G. Foti, C. Comninellis, *J. Appl. Electrochem.* **2003**, *33*, 151-154.

[5] a) J.-F. Zhi, H.-B. Wang, T. Nakashima, T. N. Rao, A. Fujishima, *J. Phys. Chem. B* **2003**, *107*, 13389-13395; b) K. E. Carter, J. Farrell, *Environ. Sci. Technol.* **2008**, *42*, 6111-6115; c) B. P. Chaplin, G. Schrader, J. Farrell, *Environ. Sci. Technol.* **2009**, *43*, 8302-8307.

[6] S. Ferro, A. De Battisti, I. Duo, C. Comninellis, W. Haenni, A. Perret, *J. Electrochem. Soc.* **2000**, *147*, 2614-2619.

[7] E. Vanhove, J. De Sanoit, J. Arnault, S. Saada, C. Mer, P. Mailley, P. Bergonzo, M. Nesladek, *Phys. Status Solidi A* **2007**, *204*, 2931-2939.

[8] a) G. Janssen, W. Van Enckevort, W. Vollenberg, L. Giling, *Diamond & Related Materials* **1992**, *1*, 789-800; b) R. Samlenski, C. Haug, R. Brenn, C. Wild, R. Locher, P. Koidl, *Diamond & Related Materials* **1996**, *5*, 947-951.

[9] L. A. Hutton, J. G. Iacobini, E. Bitziou, R. B. Channon, M. E. Newton, J. V. Macpherson, *Anal. Chem.* **2013**, *85*, 7230-7240.

[10] K. Schwarzová-Pecková, J. Vosáhlová, J. Barek, I. Šloufová, E. Pavlova, V. Petrák, J. Zavázalová, *Electrochim. Acta* **2017**, *243*, 170-182.

[11] Z. V. Živcová, O. Frank, V. Petrák, H. Tarábková, J. Vacík, M. Nesládek, L. Kavan, *Electrochim. Acta* **2013**, *87*, 518-525.

[12] J. A. Bennett, J. Wang, Y. Show, G. M. Swain, *J. Electrochem. Soc.* **2004**, *151*, E306-E313.

[13] Z. J. Ayres, J. C. Newland, M. E. Newton, S. Mandal, O. A. Williams, J. V. Macpherson, *Carbon* **2017**, *121*, 434- 442.

[14] Y. V. Pleskov, Y. E. Evstefeeva, M. Krotova, V. Varnin, I. Teremetskaya, *J. Electroanal. Chem.* **2006**, *595*, 168-174.

[15] a) R. Bogdanowicz, A. Fabiańska, L. Golunski, M. Sobaszek, M. Gnyba, J. Ryl, K. Darowicki, T. Ossowski, S. Janssens, K. Haenen, *Diamond & Related Materials* **2013**, *39*, 82-88; b) D. Becker, K. Jüttner, *J. Appl. Electrochem.* **2003**, *33*, 959-967.

[16] a) Z. V. Živcová, V. Petrák, O. Frank, L. Kavan, *Diamond & Related Materials* **2015**, *55*, 70-76; b) I. Yagi, H. Notsu, T. Kondo, D. A. Tryk, A. Fujishima, *J. Electroanal. Chem.* **1999**, *473*, 173-178.

[17] F. Liu, J. Wang, B. Liu, X. Li, D. Chen, *Diamond & Related Materials* **2007**, *16*, 454-460.

[18] a) H. V. Patten, K. E. Meadows, L. A. Hutton, J. G. Iacobini, D. Battistel, K. McKelvey, A. W. Colburn, M. E. Newton, J. V. Macpherson, P. R. Unwin, *Angew. Chem. Int. Ed.* **2012**, *51*, 7002-7006; b) H. V. Patten, S. C. Lai, J. V. Macpherson, P. R. Unwin, *Anal. Chem.* **2012**, *84*, 5427-5432; c) L. I. Tomlinson, H. V. Patten, B. L. Green, J. Iacobini, K. E. Meadows, K. McKelvey, P. R. Unwin, M. E. Newton, J. V. Macpherson, *Electroanalysis* **2016**, *28*, 2297-2302; d) H. V. Patten, L. A. Hutton, J. R. Webb, M. E. Newton, P. R. Unwin, J. V. Macpherson, *Chem. Comm.* **2015**, *51*, 164-167.

[19] a) N. Ebejer, M. Schnippering, A. W. Colburn, M. A. Edwards, P. R. Unwin, *Anal. Chem.* **2010**, *82*, 9141-9145; b) N. Ebejer, A. G. Güell, S. C. Lai, K. McKelvey, M. E. Snowden, P. R. Unwin, *Annu. Rev. Anal. Chem.* **2013**, *6*, 329-351; c) C.-H. Chen, L. Jacobse, K. McKelvey, S. C. Lai, M. T. Koper, P. R. Unwin, *Anal. Chem.* **2015**, *87*, 5782-5789.

[20] a) M. Nie, S. Neodo, J. Wharton, A. Cranny, N. Harris, R. Wood, K. Stokes, *Electrochim. Acta* **2016**, *202*, 345-356; b) A. Goodwin, A. L. Lawrence, C. E. Banks, F. Wantz, D. Omanović, Š. Komorsky-Lovrić, R. G. Compton, *Anal. Chim. Acta* **2005**, *533*, 141-145.

[21] S. P. E, Y.-R. Kim, D. Perry, C. L. Bentley, P. R. Unwin, *ACS Applied Mater. & Inter.* **2016**, *8*, 30458-30466.

[22] C. Wild, N. Herres, P. Koidl, *J. Appl. Phys.* **1990**, *68*, 973-978.

[23] M. Bernard, A. Deneuville, P. Muret, *Diamond & Related Materials* **2004**, *13*, 282-286.

[24] S. Halliwell, P. May, N. Fox, M. Othman, *Diamond & Related Materials* **2017**, *76*, 115-122.

[25] A. M. Zaitsev, *Optical properties of diamond: a data handbook*, Springer Science & Business Media, **2001**.

[26] N. Ferreira, E. Abramof, E. Corat, V. Trava-Airoldi, *Carbon* **2003**, *41*, 1301-1308.

[27] Z. J. Ayres, S. J. Cobb, M. E. Newton, J. V. Macpherson, *Electrochem. Commun.* **2016**, *72*, 59-63.

[28] N. R. Wilson, S. L. Clewes, M. E. Newton, P. R. Unwin, J. V. Macpherson, *J. Phys. Chem. B* **2006**, *110*, 5639-5646.

[29] a) G. R. Salazar-Banda, L. S. Andrade, P. A. Nascente, P. S. Pizani, R. C. Rocha-Filho, L. A. Avaca, *Electrochim. Acta* **2006**, *51*, 4612-4619; b) H. Girard, N. Simon, D. Ballutaud, M. Herlem, A. Etcheberry, *Diamond & Related Materials* **2007**, *16*, 316-325; c) G. R. Salazar-Banda, A. E. de Carvalho, L. S. Andrade, R. C. Rocha-Filho, L. A. Avaca, *J Appl. Electrochem.* **2010**, *40*, 1817-1827.

[30] a) M. C. Granger, M. Witek, J. Xu, J. Wang, M. Hupert, A. Hanks, M. D. Koppang, J. E. Butler, G. Lucazeau, M. Mermoux, *Anal. Chem.* **2000**, *72*, 3793-3804; b) M. Yoshimura, K. Honda, T. Kondo, R. Uchikado, Y. Einaga, T. N. Rao, D. Tryk, A. Fujishima, *Diamond & Related Materials* **2002**, *11*, 67-74.

[31] Y. Cai, A. B. Anderson, J. C. Angus, L. N. Kostadinov, *J. Electrochem. Soc.* **2007**, *154*, F36-F43.

[32] D. García-Osorio, R. Jaimes, J. Vazquez-Arenas, R. Lara, J. Alvarez-Ramirez, *J. Electrochem. Soc.* **2017**, *164*, E3321-E3328.

[33] a) T. Watanabe, A. Fiorani, G. Valenti, F. Paolucci, Y. Einaga, *J. Am. Chem. Soc.* **2016**, *138*, 15636-15641; b) K. Serrano, P. Michaud, C. Comninellis, A. Savall, *Electrochim. Acta* **2002**, *48*, 431-436.

[34] C. L. Bentley, D. Perry, P. R. Unwin, *Anal. Chem.* **2018**, *90*, 7700-7707.

[35] a) S. Lai, A. N. Patel, K. McKelvey, P. R. Unwin, *Angew. Chem. Int. Ed.* **2012**, *51*, 5405-5408; b) B. D. Aaronson, C.-H. Chen, H. Li, M. T. Koper, S. C. Lai, P. R. Unwin, *J. Am. Chem. Soc.* **2013**, *135*, 3873-3880.

[36] M. E. Snowden, A. G. Güell, S. C. Lai, K. McKelvey, N. Ebejer, M. A. O'Connell, A. W. Colburn, P. R. Unwin, *Anal. Chem.* **2012**, *84*, 2483-2491.

[37] L. Ostrovskaya, V. Perevertailo, V. Ralchenko, A. Dementjev, O. Loginova, *Diamond & Related Materials* **2002**, *11*, 845-850.

Entry for the Table of Contents (Please choose one layout)

Layout 1:

ARTICLE

Factors affecting solvent window: The boron doping level and surface termination are important for changing the solvent window of BDD as illustrated by correlative electrochemical microscopy (see picture).

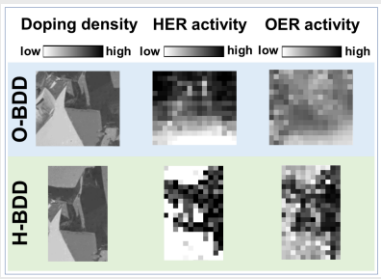

Dan-Qing Liu, Chang-Hui Chen, David Perry, Geoff West, Sam J. Cobb, Julie V. Macpherson and Patrick R. Unwin**

Page 1. – Page 7.

Facet-Resolved Electrochemistry of Polycrystalline Boron-doped Diamond Electrodes: Microscopic Factors Determining the Aqueous Solvent Window in Aqueous Potassium Chloride Solutions

Layout 2:

ARTICLE

((Insert TOC Graphic here))

*Author(s), Corresponding Author(s)**

Page No. – Page No.

Title

Text for Table of Contents